Thermochromic light scattering from particulate VO_2 layers

José Montero, Yu-Xia Ji,* Claes G. Granqvist, and Gunnar A. Niklasson

Department of Engineering Sciences, The Ångström Laboratory, Uppsala University, P. O. Box 534, SE-75121 Uppsala, Sweden

Particulate layers of thermochromic (TC) VO_2 were made by reactive DC magnetron sputtering of vanadium onto In_2O_3:Sn-coated glass. The deposits were characterized by scanning electron microscopy, atomic force microscopy and X-ray diffraction. Specular and diffuse optical transmittance and reflectance were recorded in the 300–2500-nm wavelength range and displayed pronounced TC effects. These properties could be reconciled with a semi-quantitative model based on Lorentz–Mie theory applied to the distribution of particle sizes and accounting for particle shapes by the Grenfell–Warren approach with equal-volume-to-area spheres.

.....
*E-mail: yuxia.ji@angstrom.uu.se

I. INTRODUCTION

Vanadium dioxide has thermochromic (TC) properties associated with a reversible metal–insulator transition at a "critical" temperature τ_c of about 68 °C.[1] Thin films of this material are monoclinic, semiconducting and near-infrared transparent at $\tau < \tau_c$, where τ denotes temperature, and are tetragonal, metallic-like and near-infrared-reflecting at $\tau > \tau_c$. The value of τ_c can be decreased to room temperature most easily by tungsten doping.[2,3] The TC transition is often associated with the coexistence of metallic and non-metallic regions around τ_c.[4–9] Nanoparticles of VO_2 show "nanothermochromism", and the near-infrared absorption is much smaller at $\tau < \tau_c$ than at $\tau > \tau_c$.[10,11] Thin films and nanoparticle composites of VO_2 are of considerable interest for "smart" glazings in buildings as well as for numerous other technologies.[3,12–17] Most optical applications of VO_2 require essentially non-scattering properties, and both films and nanoparticle composites have been subject to detailed studies recently.[13,15] Only a few prior investigations[9,18–25] have considered light scattering, and we particularly note recent work by Jin *et al.*[20,21] on diffuse transmittance through VO_2-based functional fiber mats and by Moot *et al.*[22] on composites of VO_2 and elastomers.

The present work considers the TC properties of particulate VO_2 deposits comprising irregular particles that are large enough to exhibit significant optical scattering, which in practice means that we deal with radii exceeding ~20 nm for the case of sphere-like objects.[26] Such particles can be prepared by many different techniques, as surveyed in earlier papers.[10,12] Here we use reactive DC magnetron sputtering, which has been found capable of making TC nanorods and nanoparticles.[12,27]

Section II below reports on the preparation of particulate VO_2 layers and of their morphological and structural characterization. Specular and diffuse optical properties are reported in Sec. III for $\tau < \tau_c$ and $\tau > \tau_c$. Section IV presents a highly simplified theoretical model for the optical properties, and this model is accompanied by a semi-quantitative analysis and comparison with experimental data in Sec. V. Comments and conclusions are given in Sec. VI.

II. PREPARATION OF PARTICULATE VO_2 FILMS AND THEIR MORPHOLOGICAL AND STRUCTURAL CHARACTERIZATION

Thin layers of VO_2 were prepared by reactive DC magnetron sputtering in a deposition system based on a Balzers UTT 400 unit from a 5-cm-diameter metallic vanadium disc (99.5% pure) at a sputtering power P. The deposition chamber was first evacuated to a base pressure of 6.3×10^{-7} mbar, and the pressure was then set to 1.2×10^{-2} mbar by introducing a working gas (Ar) mixed with a reactive gas (O_2). The mixing ratio Γ is defined as

$$\Gamma = [\phi_{O2}/(\phi_{Ar} + \phi_{O2})], \quad (1)$$

where ϕ_{O2} and ϕ_{Ar} are oxygen and argon fluxes, respectively. The substrates were 1-mm-thick glass plates pre-coated with In_2O_3:Sn (known as ITO) having a resistance/square of 60 Ω (manufactured by Colorado Concept Coating LLD, Loveland, CO, USA). According to our previous studies[27] ITO promotes the crystallinity of VO_2 deposits and, under certain conditions, induces the growth of highly particulate samples.

For the present work, a high substrate temperature (450 ± 10 ºC) was used and deposition occurred under oxidizing conditions, accomplished by having a large value of Γ. Specifically, P was fixed at 8.58 W/cm^2 and VO_2-rich samples were then formed for $5.25 < \Gamma < 6.40\%$;[22] the growth of particulate films took place at $\Gamma \geq 5.9\%$. The V_2O_5 content tended to rise as Γ was increased, which led to a gradual deterioration of the TC behavior especially for $\Gamma > 6.4\%$. Hence a compromise must be reached, and Γ should be high enough to accomplish particle growth but low enough to maintain VO_2-stoichiometry. On this basis, $\Gamma = 5.9\%$ as an optimum value was selected for the deposition of particulate TC samples. Our investigation encompassed 12 samples.

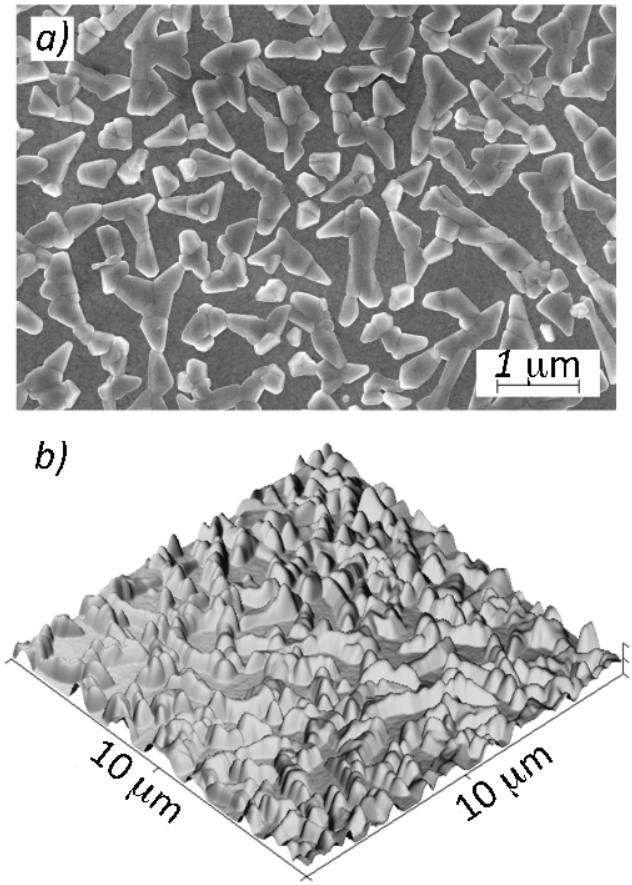

FIG. 1. (a) SEM micrograph of a typical VO_2 sample deposited onto ITO-coated glass. (b) AFM image for the same sample; the vertical scale extends from zero to 190 nm.

Structural characterization of the deposits was performed by use of a LEO 1550 FEG Gemini Scanning Electron Microscope (SEM) operating at an acceleration voltage of 5 kV. Figure 1(a) shows a representative SEM micrograph of a particulate sample displaying irregular μm-size objects with well-defined boundaries. Surface morphology was studied with a Veeco Dimension^{TM} 3100 Atomic Force Microscope (AFM) (tip radius 50 nm, spring constant 5 N/m, and resonance frequency 74 kHz). Figure 1(b) is a "three-dimensional" AFM plot of a 10 × 10 μm^2 surface area approximately half of which is covered by particles. The total volume of the nanostructures is ~4.5 μm^3, the maximum peak height is ~190 nm, and the root-mean-square

surface roughness is ~40 nm. Particle volumes V_p and surface areas S_p were extracted from AFM data using "Gwyddion" open-source software[28] and will be presented and discussed in Sec. V.

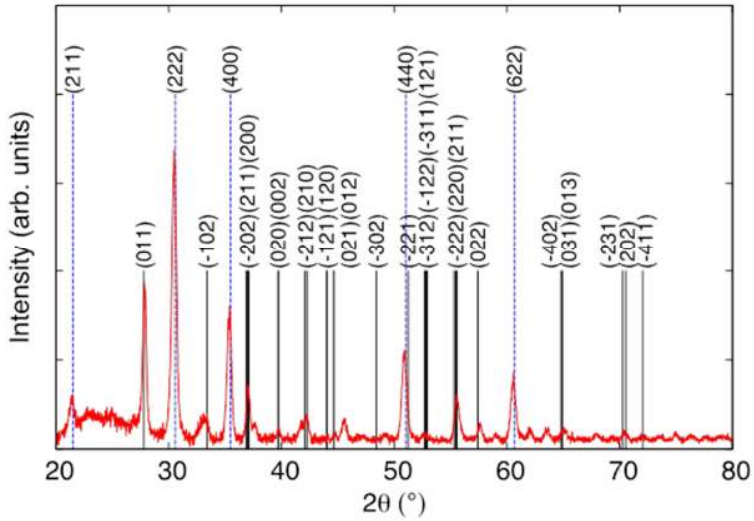

FIG. 2. GIXRD data, showing diffracted intensity *vs*. diffraction angle 2θ, taken at room temperature for the VO_2 sample shown in Fig. 1. Vertical solid lines indicate the shown reflections in monoclinic VO_2, and vertical dashed lines refer to reflections in ITO.

The crystalline structure of the VO_2 samples was analyzed by grazing incidence x-ray diffraction (GIXRD), using a Siemens D5000 θ–2θ instrument, for diffraction angles in the $20 \leq 2\theta \leq 80°$ range and at room temperature. The data in Fig. 2 show multiple peaks emanating from VO_2 and ITO. For VO_2, the identification of Miller indices made by Li *et al.*[12] was followed and our data were found to be consistent with monoclinic VO_2 according to the Joint Committee on Powder Diffraction Standards (JCPDS) Card 00-043-1051. Other peaks could be assigned to ITO and agree with JCPDS card 00-006-0416. A more detailed discussion of GIXRD data was given in an earlier paper.[27]

III. OPTICAL CHARACTERIZATION

Spectral optical properties of nanostructured VO_2 samples were determined in the $300 \leq \lambda \leq 2500$ nm wavelength range by use of a Perkin-Elmer Lambda 900 spectrophotometer equipped with an integrating sphere and a custom-built heating accessory incorporating a resistive thermometer. Data were taken at $\tau_c > \tau \approx 20$ °C and $\tau_c < \tau \approx 100$ °C, *i.e.*, with the sample in

semiconducting (sc) and metallic (m) state, respectively. Both specular (spec) and diffuse (diff) transmittance T and reflectance R were recorded; the methods are discussed in more detail elsewhere.[29,30] Total transmittance is given by

$$T_{tot} = T_{spec} + T_{diff} \quad , \tag{2}$$

and an analogous expression holds for R_{tot}.

Figure 3 illustrates T_{tot} *vs*. temperature at ~30 < τ < 75 °C and λ = 2000 nm for the sample reported on above. Heating and cooling took place at ~1.5 °C/minute. Clearly the transmittance shifts reversibly between ~75 and 32% when the temperature is altered. The change is centered at ~58 °C and differs by ~17 °C between heating and cooling. A transition width of this order of magnitude is not unexpected and, for example, some VO_2 films made recently by physical vapor deposition yielded somewhat narrower transitions[31,32] whereas films prepared by chemical vapor deposition showed broader transitions.[16]

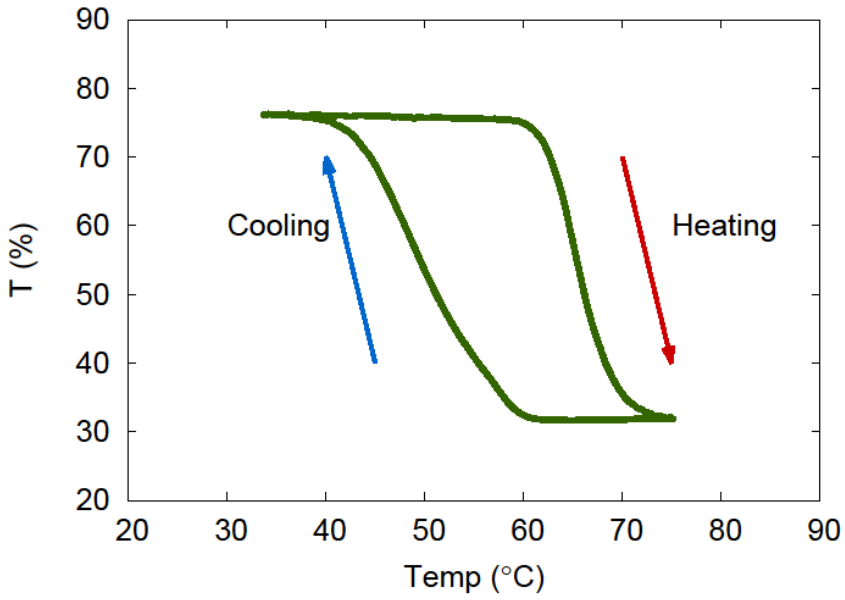

FIG. 3. Temperature dependent total optical transmittance T at a wavelength of 2000 nm for the particulate VO_2 sample presented in Fig. 1. Arrows indicate heating and cooling.

Figures 4(a) and 4(b) show data on specular properties ($T^{sc}_{spec}, T^{m}_{spec}, R^{sc}_{spec}, R^{m}_{spec}$) and diffuse properties ($T^{sc}_{diff}, R^{sc}_{diff}, T^{m}_{diff}, R^{m}_{diff}$), respectively. The specular transmittance displays clear TC performance and is larger in the semiconducting state than in the metallic state for λ > 1100 nm, whereas the opposite holds true for shorter wavelengths. The specular reflectance lies consistently at <10%. The plateau in T_{spec} at λ ~ 400 nm ensues from the difference in optical band gaps for VO_2 and ITO. The diffuse optical properties show TC properties as well, and the transmittance, which is peaked at λ ~ 500 nm, is consistently larger in the semiconducting state than in the metallic state. The diffuse reflectance displays an interesting behavior and is larger in the metallic state than in the semiconducting state for λ > 1300 nm, whereas the opposite is true for λ < 1300 nm.

In order to be able to discuss the optical properties in terms of theory below, the data of T and R were converted to extinction-, absorption- and scattering coefficients denoted α_{ext}, α_{abs}, and α_{sca}, respectively. Extinction is the sum of absorption and scattering, and hence the respective coefficients are related by

$$\alpha_{ext} = \alpha_{abs} + \alpha_{sca} \, . \tag{3}$$

A number of assumptions are necessary in order to obtain the coefficients from experimental data. First the VO_2 particle layer is treated as a homogeneous film with effective optical parameters; this approximation has been found to work well for discontinuous metal films.[33] Secondly, the optical density of a thin non-scattering film on a transparent substrate can be obtained with good accuracy from the logarithm of the so called "special absorption" defined by $(1 - R)/T$, as shown by Hong.[34] Thirdly, our particle films are scattering and hence their optical density has contributions from both absorption and scattering and is equal to $\alpha_{ext}d$, where d represents the thickness of the particle layer. Thus the extinction coefficient can be obtained from measurements of specular transmittance and reflectance by

$$\alpha_{ext} \approx -\frac{1}{d} \ln\left(\frac{T_{spec}}{1-R_{spec}}\right) . \tag{4}$$

On the other hand, the total transmittance and reflectance have contributions from both directly transmitted and reflected light as well as scattered light. An optical density calculated from the total quantities would then depend solely on the absorption in the particle layer. Hence we

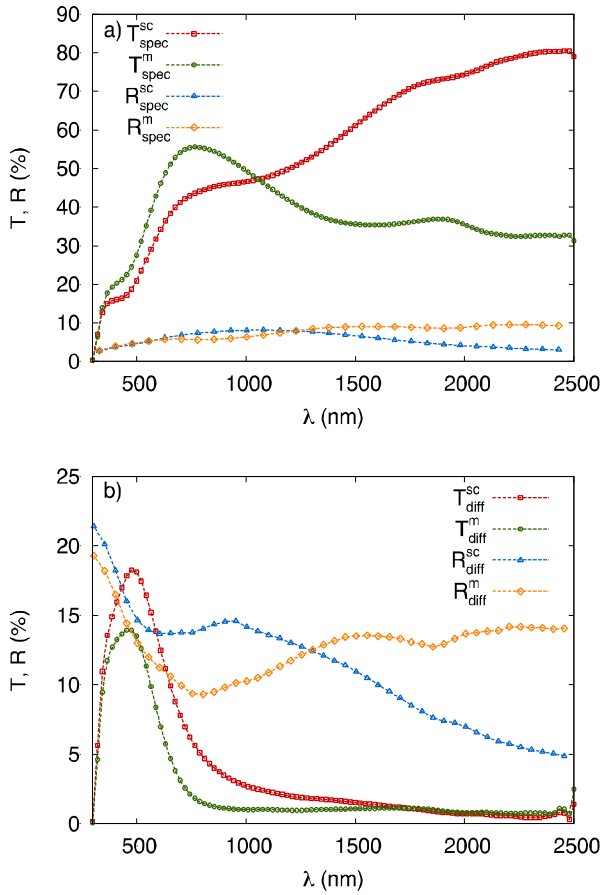

FIG. 4. (a) Specular (spec) and (b) diffuse (diff) transmittance T and reflectance R of the particulate VO_2 sample presented in Fig. 1. Data are shown for the semiconducting (sc) state at $\tau < \tau_c$ and the metallic (m) state at $\tau > \tau_c$.

propose that a relationship analogous to Eq. (4) connects the absorption coefficient to T_{tot} and R_{tot} by

$$\alpha_{\mathrm{abs}} \approx -\frac{1}{d}\ln\left(\frac{T_{\mathrm{tot}}}{1-R_{\mathrm{tot}}}\right). \tag{5}$$

The scattering coefficient is then obtained from Eq. (3). Finally, d is identified with the maximum peak height obtained by AFM.

IV. PRELIMINARY OPTICAL MODELLING

It is instructive to first carry out a simple modelling of optical cross-sections for a single VO_2 sphere at $\tau < \tau_c$ and $\tau > \tau_c$. This can be done with particle radius r_p as parameter by use of Lorenz–Mie theory, which is applicable in the entire wavelength range irrespectively of the magnitude of r_p.[35,36] Scattering and extinction cross sections can be expressed as

$$C_{\mathrm{sca}} = \left(\frac{2\pi r_p^2}{x^2}\right)\sum_{n=1}^{\infty}(2n+1)(|a_n|^2 + |b_n|^2) \tag{6}$$

and

$$C_{\mathrm{ext}} = \left(\frac{2\pi r_p^2}{x^2}\right)\sum_{n=1}^{\infty}(2n+1)[Re(a_n + b_n)] \tag{7}$$

respectively, where $x = 2\pi n_m r_p/\lambda$ is a size parameter and the Mie coefficients a_n and b_n are obtained from the boundary conditions at the sphere's surface. The absorption cross section C_{abs} is obtained from the difference between the extinction and scattering cross sections. Specifically, we employed computer code from Bohren and Huffman[37] together with data on the complex refractive index of the particles n_p and of their surrounding medium n_m. We used n_p from recent data extracted from spectrophotometric measurements on VO_2 films by Li *et al.*[20] and set $n_m = 1$ corresponding to air. Given these parameters, the program computes C_{sca} and C_{abs}, as shown above. Scattering and absorption cross-section per unit volume unit, denoted C^*_{sca} and C^*_{abs}, respectively, are obtained from

$$C^*_{\mathrm{sca(abs)}} = \frac{C_{\mathrm{sca(abs)}}}{V_p} \tag{8}$$

where V_p is the particle volume.

Figure 5 shows data on C^*_{sca} calculated for semiconducting and metallic spherical VO_2 particles with $70 \leq r_p \leq 500$ nm, surrounded by air, and establishes the basics for temperature dependent modulation of C^*_{sca} and hence of TC light scattering by spherical VO_2 particles. The color-coding in Fig. 5 expresses the magnitude of C^*_{sca} as a function of r_p: as expected, scattering features in the infrared ($\lambda > 700$ nm) are dominated by the larger spheres with $200 < r_p \leq 500$ nm, while scattering in the visible spectral region ($400 < \lambda < 700$ nm) is dominated by smaller spheres with $70 \leq r_p < 200$ nm. Interestingly, there are significant differences in the sign of the TC modulation depending on sphere radius and, for example, $C^{*\mathrm{m}}_{\mathrm{sca}} > C^{*\mathrm{sc}}_{\mathrm{sca}}$ for $r_p \lesssim 100$ nm and

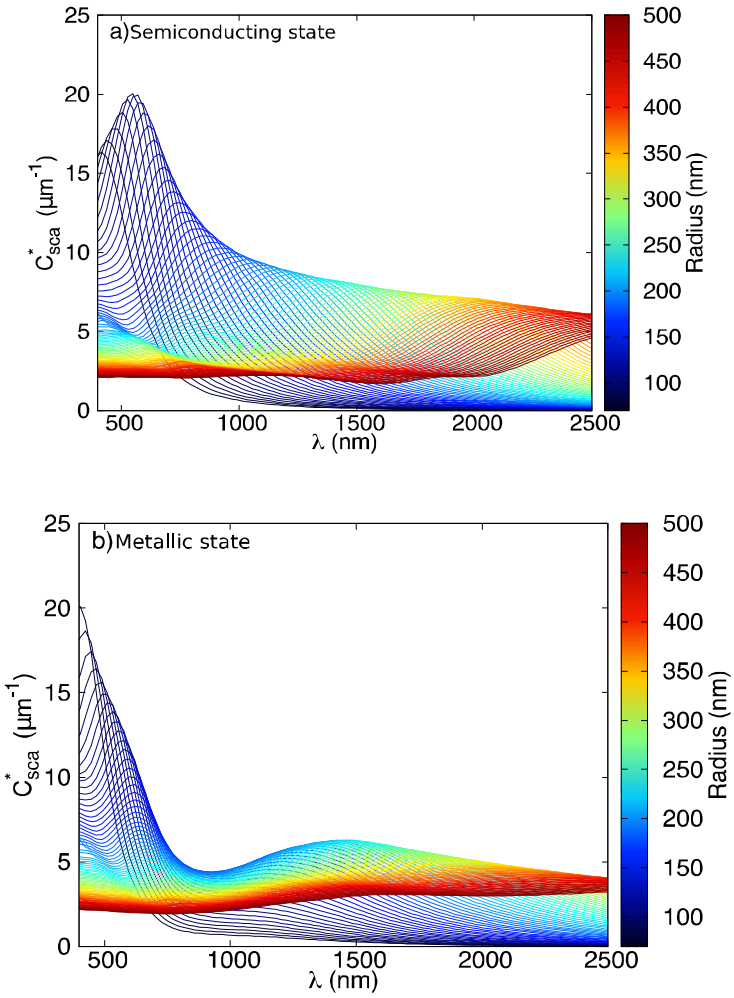

FIG. 5. Spectral scattering cross-section per unit volume calculated from Lorenz–Mie theory for VO_2 spheres of different radii (reported for 5 nm increments). Data are shown for VO_2 in (a) semiconducting state at $\tau < \tau_c$ and in (b) metallic state at $\tau > \tau_c$.

for the shortest wavelengths, while $C_{\mathrm{sca}}^{*\mathrm{m}} < C_{\mathrm{sca}}^{*\mathrm{sc}}$ or $C_{\mathrm{sca}}^{*\mathrm{m}} > C_{\mathrm{sca}}^{*\mathrm{sc}}$, depending on wavelength, for $r_p \gtrsim 100$ nm. Figure 5 leads to the conclusion that significant TC modulation of light scattering, especially at $500 < \lambda < 1000$ nm, can be achieved by use of spherical VO_2 particles with $r_p \lesssim 200$ nm.

V. SEMI-QUANTITATIVE OPTICAL MODELLING, AND COMPARISON WITH EXPERIMENTAL DATA

The Lorenz–Mie model, presented above, is valid for a single spherical particle. However, Eq. (8) can be readily generalized to obtain effective scattering and absorption coefficients of a particle layer by the relation

$$K^*_{\mathrm{sca(abs)}} = \int_0^\infty N(r)\, C_{\mathrm{sca(abs)}}(r)\, dr \quad , \tag{9}$$

where $K^*_{\mathrm{sca(abs)}}$ is the scattering (absorption) coefficient, *i.e.*, the cross-section per volume unit for a distribution of spherical particles of radius r, characterised by their number density $N(r)$. Such a distribution is appropriate in our case, except that the samples are comprised of non-spherical particles.

Deviations from spherical shapes can be handled in different ways. A straight-forward approach is to introduce equal-volume spheres, *i.e.*, representing a particle of volume V_p by an equivalent sphere of radius r_{eq} according to

$$r_{\mathrm{eq}} = \left[\frac{3V_p}{4\pi}\right]^{\frac{1}{3}} . \tag{10}$$

It should be noted that an equal-volume sphere normally has a much smaller projected surface than the actual particle it represents. This description preserves the number of particles in the studied sample.

An alternative method to account for non-spherical shapes was put forward by Grenfell and Warren[38] who demonstrated that non-spherical particles of volume V_p and surface area S_p could be adequately represented as a collection of volume-to-area spheres of equivalent radius r'_{eq} given by

$$r'_{\mathrm{eq}} = 3\frac{V_p}{S_p} . \tag{11}$$

Both volume and surface area are preserved in this model, and the number of spheres representing an actual irregular particle is $3V_p/4\pi(r'_{\mathrm{eq}})^3$; hence the number of particles is not preserved.

In the calculation of $K^*_{\mathrm{sca(abs)}}$ represented by Eq. (9), $N(r)$ should be substituted by the equivalent number densities $N_{\mathrm{eq}}(r_{\mathrm{eq}})$ or $N_{\mathrm{eq}}(r'_{\mathrm{eq}})$ pertinent to the equal-volume or equal-volume-to-area approximations, respectively. Figure 6 shows such data derived from the AFM image of the 10 × 10 μm^2 surface presented in Fig. 1(b). This surface includes ~460 non-spherical particles that can be represented by either the same number of equal-volume spheres or by 2175 equal-volume-to-area spheres. The two sets of data are very different, and the equal-volume-to-area spheres have a rather narrow distribution peaked at $r'_{\mathrm{eq}} \approx 65$ nm whereas the equal-volume spheres display a broad and skewed distribution with a peak at $r_{\mathrm{eq}} \approx 100$ nm.

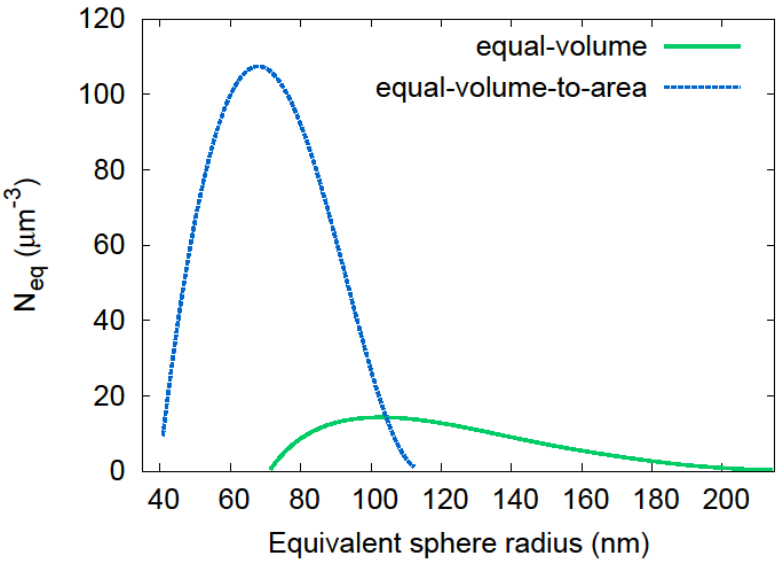

FIG. 6. Normalized distributions of the number of equivalent spheres with different radii r_{eq} or r_{eq}' calculated using the equal-volume and equal-volume-to-area ratio approximations, respectively. The analysis is based on the AFM data in Fig. 1(b).

Figure 7 reports computed data on K^*_{abs} and K^*_{sca} for a particulate VO_2 sample in semiconducting and metallic states and using the distributions in Fig. 6. The data are compared with corresponding experimental results for α_{abs} and α_{sca}. The spectral interval is $400 \leq \lambda \leq 1000$ nm for absorption data and for $400 \leq \lambda \leq 2500$ nm for scattering; the former of these ranges avoids

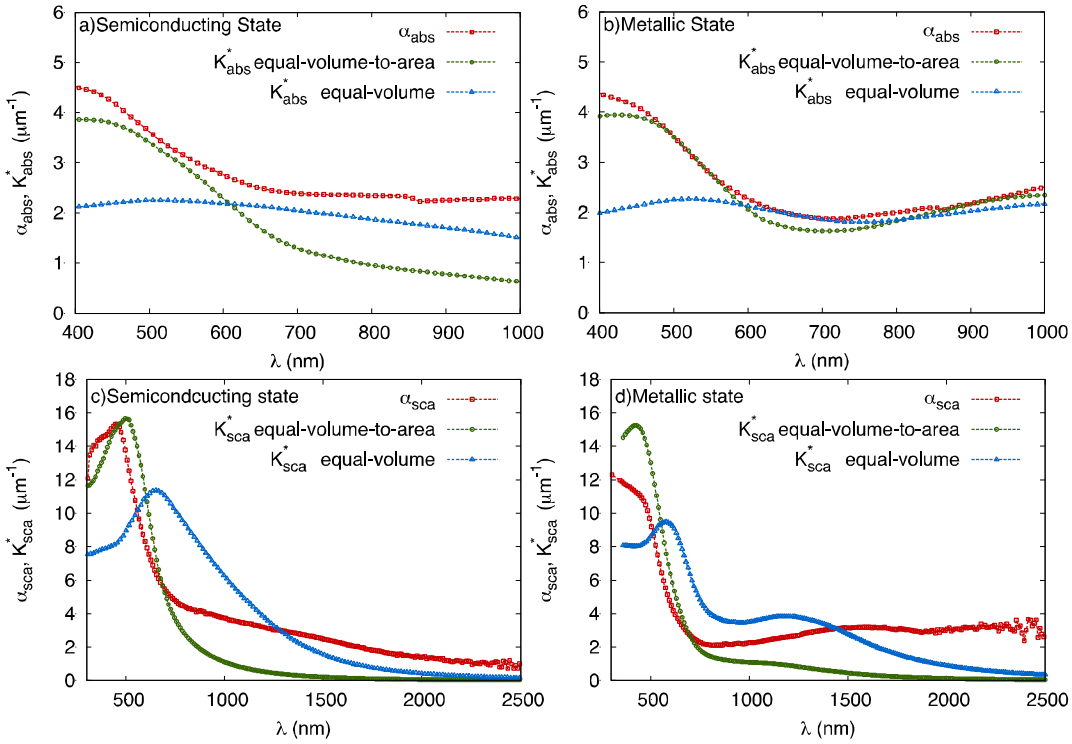

FIG. 7. Experimental (α_{abs}) and theoretical (K^*_{abs}) spectral absorption data calculated according to the equal-volume and equal-volume-to-area approximations, and corresponding results for experimental (α_{sca}) and theoretical (K^*_{sca}) spectral scattering data, for the VO_2 sample depicted in Fig. 1. Data are reported for the semiconducting state at $\tau < \tau_c$ [panels (a) and (c)] and the metallic state at $\tau > \tau_c$ [panels (b) and (d)].

obscuring effects of absorption in the ITO layer. It is clear that the approximation with equal-volume-to-area spheres can be reconciled with the experimental data for $\lambda < 700$ nm as regards absorption as well as scattering and at both low and high temperature. The discrepancies at larger wavelengths are not unexpected considering the fact that the values of r'_{eq} are considerably smaller than the measured particle sizes. The approximation with equal-volume spheres is clearly less successful.

VI. COMMENTS AND CONCLUSIONS

Layers of irregular thermochromic VO_2 particles were prepared by reactive sputtering onto heated ITO-coated glass. Particle morphology was characterized by SEM and AFM. Optical specular and diffuse transmittance and reflectance were recorded in the 300–2500-nm spectral range, encompassing visible light and solar radiation, and displayed pronounced thermochromic

effects for specular transmittance and for diffuse transmittance and reflectance. These optical properties could be reconciled with a semi-quantitative model based on Lorenz–Mie theory[34,35] applied to an experimentally determined distribution of particle sizes and accounting for particle shapes by the Grenfell–Warren approach[38] with equal-volume-to-area spheres. The model was particularly successful for visible wavelengths. Preliminary analyses of other samples, comprising particles of different shapes, rendered support to the results of the present paper.

The explorative character of the present work, and several uncertainties in the analytic approach, should be recognized. The derivations of extinction- and absorption coefficient from spectral data on specular and total transmittance and reflectance are approximative, especially as regards the absorption coefficient, and the representation of the particles in terms of equal-volume-to-area spheres is far from unique. Considering these unavoidable approximations, it is gratifying—possibly even surprising—that the essentials of the experimental data can be satisfactorily captured by theory. Further refinement of the theoretical modelling is an outstanding challenge for future work.

As a general conclusion, we observe that our work opens experimental and theoretical avenues to explore thermochromic light scattering, which may be of interest for applications in optical technology. Two examples that has attracted some interest recently concern diffuse transmittance through VO_2-based functional fiber mats[20,21] and composites of VO_2 and elastomers.[22]

ACKNOWLEDGMENTS

Financial support was received from the Swedish Research Council for Environment, Agricultural Sciences and Spatial Planning (Formas) and from the European Research Council under the European Community's Seventh Framework Program (FP/2007–2013)/ERC Grant Agreement No. 267234 (GRINDOOR).

REFERENCES

[1]F. J. Morin, Phys. Rev. Lett. **3**, 34 (1959).

[2]J. B. Goodenough, J. Solid State Chem. **3**, 490 (1971).

[3]S.-Y. Li, G. A. Niklasson, and C. G. Granqvist, Thin Solid Films **520**, 3823 (2012).

[4]M. M. Qazilbash, A. Tripathi, A. A. Schafgans, B.-J. Kim, H.-T. Kim, Z. Cai, M. V. Holt, J. M. Maser, F. Keilmann, O. G. Shpyrko, and D. N. Basov, Phys. Rev. B **83**, 165108 (2011).

[5]M. M. Qazilbash, M. Brehm, B.-G. Chae, P.-C. Ho, G. O. Andreev, B.-J. Kim, S. J. Yun, A. V. Balatsky, M. B. Maple, F. Keilmann, H.-T. Kim, and D. N. Basov, Science **318**, 1750 (2007).

[6]M. M. Qazilbash, M. Brehm, G. O. Andreev, A. Frenzel, P. C. Ho, B.-G. Chae, B.-J. Kim, S. J. Yun, H.-T. Kim, A. V. Balatsky, O. G. Shpyrko, M. B. Maple, F. Keilmann, and D. N. Basov, Phys. Rev. B **79**, 075107 (2009).

[7]Z. Topalian, S.-Y. Li, G. A. Niklasson, C. G. Granqvist, and L. B. Kish, J. Appl. Phys. **117**, 025303 (2015).

[8]H. Madan, M. Jerry, A. Pogrebnyakov, T. Mayer, and S. Datta, ACS Nano **9**, 2009 (2015).

[9]S. Kumar, J. P. Strachan, A. L. D. Kilcoyne, T. Tyliszcak, M. D. Pickett, C. Santori, G. Gibson, and R. S. Williams, arXiv:1512.08921 [Appl. Phys. Lett. (2016)].

[10]S.-Y. Li, G. A. Niklasson, and C. G. Granqvist, J. Appl. Phys. **108**, 063525 (2010).

[11]S.-Y. Li, G. A. Niklasson, and C. G. Granqvist, J. Appl. Phys. **109**, 113515 (2011).

[12]S.-Y. Li, K. Namura, M. Suzuki, G. A. Niklasson, and C. G. Granqvist, J. Appl. Phys. **114**, 033516 (2013).

[13]Z. Chen, Y. Gao, L. Kang, C. Cao, S. Chen, and H. Luo, J. Mater. Chem. A **2**, 2718 (2014).

[14]C. G. Granqvist, J. Vac. Sci. Technol. B **32**, 060801 (2014).

[15]S. Hoffmann, E. S. Lee, and C. Clavero, Sol. Energy Mater. Sol. Cells **123**, 65 (2014).

[16]M. E. A. Warwick and R. Binions, J. Mater. Chem. A **2**, 3275 (2014).

[17]S.-Y. Li, G. A. Niklasson, and C. G. Granqvist, J. Appl. Phys. **115**, 053513 (2014).

[18]O. P. Mikheeva and A. I. Sidorov, Zh. Tekh. Fiz. **73**, 79 (2003) [English translation Tech. Phys. **48,** 602 (2003)].

[19]S. Li, Y. Li, M. Jiang, S. Ji, H. Luo, Y. Gao, and P. Jin, ACS Appl. Mater. Interfaces **5**, 6453 (2013).

[20]S. Li, Y. Li, K. Qian, S. Ji, H. Luo, Y. Gao, and P. Jin, ACS Appl. Mater. Interfaces **6**, 9 (2014).

[21]K. Qian, S. Li, S. Ji, W. Li, Y. Li, R. Chen, and P. Jin, Ceram. Int. **40**, 14517 (2014).

[22]T. Moot, C. Palin, S. Mitran, J. F. Cahoon, and R. Lopez, Adv. Opt. Mater. DOI: 10.1002/adom.201500586.

[23]S. Lysenko, F. Fernández, A. Rúa, J. Aparico, N. Sepúlveda, J. Figueroa, K. Vargas, and J. Cordero, J. Appl. Phys. **117**, 184304 (2015).

[24]S. Lysenko, F. Fernández, A. Rúa, N. Sepúlveda, and J. Aparico, Appl. Opt. **54**, 2141 (2015).

[25]M. Sullivan, T. V. Son, N. Beaudoin, and A. Haché, Opt. Commun. **356**, 395 (2015).

[26]K. Laaksonen, S. Y. Li, S. R. Puisto, N. K. J. Rostedt, T. Ala-Nissila, C. G. Granqvist, R. M. Nieminen, and G. A. Niklasson, Sol. Energy Mater. Sol. Cells **130**, 132 (2014).

[27]J. Montero, Y.-X. Ji, S.-Y. Li, G. A. Niklasson, and C. G. Granqvist, J. Vac. Sci. Technol. B **33**, 031805 (2015).

[28]D. Nečas and P. Klapetek, Centr. Eur. J. Phys. **10**, 181 (2012).

[29]D. Barrios, R. Vergaz, J. M. Sanchez-Pena, C. G. Granqvist, and G. A. Niklasson, Sol. Energy Mater. Sol. Cells **111**, 115 (2013).

[30]D. Barrios, R. Vergaz, J. M. Sánchez-Pena, B. García-Cámara, C. G. Granqvist, and G. A. Niklasson, Sol. Energy Mater. Sol. Cells **143**, 613 (2015).

[31]J.-P. Fortier, B. Baloukas, O. Zabeida, J. E. Klemberg-Sapieha, and L. Martinu, Sol. Energy Mater. Sol. Cells 125, 291 (2014).

[32]A. Aijaz, Y.-X. Ji, J. Montero, G. A. Niklasson, C. G. Granqvist, and T. Kubart, Sol. Energy Mater. Sol. Cells, to be published (2016).

[33]T. V. Amotchkina, M. K. Trubetskov, A. V. Tikhonravov, V. Janicki, J. Sancho-Parramon, and H. Zorc, Appl. Opt. **50**, 6189 (2011).

[34]W. Q. Hong, J. Phys. D: Appl. Phys. **22**, 1384 (1989).

[35]H. Valentiner, *Ouvres Scientifiques de L. Lorenz* (Lehmann & Stage, Copenhagen, Denmark, 1898).

[36]G. Mie, Ann. Phys. **330**, 377 (1908).

[37]C. F. Bohren and D. R. Huffman, *Absorption and Scattering of Light by Small Particles* (Wiley, New York, 1983).

[38]T. C. Grenfell and S. G. Warren, J. Geophys. Res.: Atm. **104**, 31697 (1999).